REPORT DOCUMENTATION PAGE

Form Approved OMB NO. 0704-0188

1. REPORT DATE (DD-MM-YYYY)	2. REPORT TYPE	3. DATES COVERED (From - To)
07-01-2015	Final Report	1-May-2011 - 30-Apr-2014

4. TITLE AND SUBTITLE

Final Report: Theoretical Design and Experimental Evaluation of Molten Carbonate Modified LSM Cathode for Low Temperature Solid Oxide Fuel Cells

5a. CONTRACT NUMBER
W911NF-11-1-0151

5b. GRANT NUMBER

5c. PROGRAM ELEMENT NUMBER
206022

6. AUTHORS

Changyong Qin, Kevin Huang

5d. PROJECT NUMBER

5e. TASK NUMBER

5f. WORK UNIT NUMBER

7. PERFORMING ORGANIZATION NAMES AND ADDRESSES

Benedict College
Office of Research
1600 Harden St.
Columbia, SC 29204 -1058

8. PERFORMING ORGANIZATION REPORT NUMBER

9. SPONSORING/MONITORING AGENCY NAME(S) AND ADDRESS (ES)

U.S. Army Research Office
P.O. Box 12211
Research Triangle Park, NC 27709-2211

10. SPONSOR/MONITOR'S ACRONYM(S)
ARO

11. SPONSOR/MONITOR'S REPORT NUMBER(S)
59047-CH-REP.29

12. DISTRIBUTION AVAILIBILITY STATEMENT

Approved for Public Release; Distribution Unlimited

13. SUPPLEMENTARY NOTES

The views, opinions and/or findings contained in this report are those of the author(s) and should not contrued as an official Department of the Army position, policy or decision, unless so designated by other documentation.

14. ABSTRACT

Using DFT and experimental methods, the following topics have been deeply explored. (1) Interaction between oxygen and molten carbonate; (2) Fabrication and test of SOFCs with MC modified LSM cathodes; (3) Low-temperature SOFCs using MC modified LSCF/GDC cathode; (4) Spectroscopic and DFT evidence of pyrocarbonate. The results point out that molten carbonate modified cathodes can significantly reduce the operating temperature of SOFCs by enhancing the ORR process at low temperatures of 500-650C. The mechanism of ORR with the presence of MC was proposed through DFT modeling and the theoretical results agree well with the

15. SUBJECT TERMS

Solid Oxide Fuel Cell, Oxygen Reduction, Molten Carbonate, Cathode Reaction, DFT Modeling

16. SECURITY CLASSIFICATION OF:			17. LIMITATION OF ABSTRACT	15. NUMBER OF PAGES	19a. NAME OF RESPONSIBLE PERSON
a. REPORT	b. ABSTRACT	c. THIS PAGE			Changyong Qin
UU	UU	UU	UU		19b. TELEPHONE NUMBER 803-705-4582

Report Title

Final Report: Theoretical Design and Experimental Evaluation of Molten Carbonate Modified LSM Cathode for Low Temperature Solid Oxide Fuel Cells

ABSTRACT

Using DFT and experimental methods, the following topics have been deeply explored. (1) Interaction between oxygen and molten carbonate; (2) Fabrication and test of SOFCs with MC modified LSM cathodes; (3) Low-temperature SOFCs using MC modified LSCF/GDC cathode; (4) Spectroscopic and DFT evidence of pyrocarbonate. The results point out that molten carbonate modified cathodes can significantly reduce the operating temperature of SOFCs by enhancing the ORR process at low temperatures of 500-650C. The mechanism of ORR with the presence of MC was proposed through DFT modeling and the theoretical results agree well with the experiments.

Enter List of papers submitted or published that acknowledge ARO support from the start of the project to the date of this printing. List the papers, including journal references, in the following categories:

(a) Papers published in peer-reviewed journals (N/A for none)

Received		Paper
08/30/2012	3.00	Nansheng Xu, Xue Li, Siwei Wang, Kevin Huang, William H. Harris, Wilson K. S. Chiu, Lingling Zhang. High CO2 permeation flux enabled by highly interconnected three-dimensional ionic channels in selective CO2 separation membranes, Energy & Environmental Science, (06 2012): 0. doi: 10.1039/c2ee22045h
08/30/2012	4.00	Arianna Gladney. Sensitivity of the C-N Vibration to Solvation in Dicyanobenzenes: A DFT Study, Open Journal of Physical Chemistry, (02 2012): 117. doi: 10.4236/ojpc.2012.22016
08/31/2013	11.00	X. Li, Y. Gong, L. Zhang, W. Tharp, C. Qin, K. Huang. Molten Carbonates as an Effective Oxygen Reduction Catalyst for 550-650 C Solid Oxide Fuel Cells, Journal of the Electrochemical Society, (06 2013): 0. doi: 10.1149/2.031309jes
08/31/2013	12.00	Lingling Zhang, Xinyu Huang, Changyong Qin, Kyle Brinkman, Yunhui Gong, Siwei Wang, Kevin Huang. First spectroscopic identification of pyrocarbonate for high CO2 flux membranes containing highly interconnected three dimensional ionic channels, Physical Chemistry Chemical Physics, (06 2013): 0. doi: 10.1039/c3cp52362d
08/31/2013	13.00	Diego Palacio, Yunhui Gong, Xueyan Song, Rajankumar L. Patel, Xinhua Liang, Xuan Zhao, John B. Goodenough, Kevin Huang. Stabilizing Nanostructured Solid Oxide Fuel Cell Cathode with Atomic Layer Deposition, Nano Letters, (08 2013): 0. doi: 10.1021/nl402138w
09/05/2013	20.00	Y. Gong, C. Qin, K. Huang. Can Silver Be a Reliable Current Collector for Electrochemical Tests?, ECS Electrochemistry Letters, (11 2012): 0. doi: 10.1149/2.010301eel
09/09/2014	21.00	Yunhui Gong, Rajankumar L. Patel, Xinhua Liang, Diego Palacio, Xueyan Song, John B. Goodenough, Kevin Huang. Atomic Layer Deposition Functionalized Composite SOFC Cathode La, Chemistry of Materials, (11 2013): 0. doi: 10.1021/cm402879r
09/09/2014	22.00	Yunhui Gong, Kevin Huang. Study of a renewable biomass fueled SOFC: The effect of catalysts, International Journal of Hydrogen Energy, (12 2013): 0. doi: 10.1016/j.ijhydene.2013.05.147
09/09/2014	23.00	Y. Gong, X. Li, L. Zhang, W. Tharp, C. Qin, K. Huang. Promoting Electrocatalytic Activity of a Composite SOFC Cathode La0.8Sr0.2MnO3+ /Ce0.8Gd0.2O2- with Molten Carbonates, Journal of the Electrochemical Society, (12 2013): 0. doi: 10.1149/2.034403jes
09/09/2014	24.00	Lingling Zhang, Jingjing Tong, Yunhui Gong, Minfang Han, Siwei Wang, Kevin Huang. Fast electrochemical CO2 transport through a dense metal-carbonate membrane: A new mechanistic insight, Journal of Membrane Science, (10 2014): 0. doi: 10.1016/j.memsci.2014.06.028
09/09/2014	25.00	Lingling Zhang, Yunhui Gong, Jacob Yaggie, Siwei Wang, Kevin Romito, Kevin Huang. Surface modified silver-carbonate mixed conducting membranes for high flux CO2 separation with enhanced stability, Journal of Membrane Science, (03 2014): 0. doi: 10.1016/j.memsci.2013.10.067
TOTAL:	**11**	

Number of Papers published in peer-reviewed journals:

(b) Papers published in non-peer-reviewed journals (N/A for none)

Received	Paper

TOTAL:

Number of Papers published in non peer-reviewed journals:

(c) Presentations

Number of Presentations: 5.00

Non Peer-Reviewed Conference Proceeding publications (other than abstracts):

Received	Paper

TOTAL:

Number of Non Peer-Reviewed Conference Proceeding publications (other than abstracts):

Peer-Reviewed Conference Proceeding publications (other than abstracts):

Received	Paper	
08/29/2012	2.00	Xue Li, Guoliang Xiao, Seung Min Lee, Kevin Huang. Mixed Oxide-Ion and Carbonate-Ion Conductors (MOCCs) as Electrolyte Materials for Solid Oxide Fuel Cells, 218th ECS Meeting. 15-AUG-11, Las Vegas, NV. : ,

TOTAL: **1**

Number of Peer-Reviewed Conference Proceeding publications (other than abstracts):

(d) Manuscripts

Received	Paper	
08/30/2012	6.00	Changyong Qin, Arianna Gladney. DFT Study of CO$_{4}^{2-}$ and CO$_{5}^{2-}$ Relevant to Oxygen Reduction with the Presence of Molten Carbonate in Solid Oxide Fuel Cells, Computational and Theoretical Chemistry (06 2012)
TOTAL:	**1**	

Number of Manuscripts:

Books

Received	Book
TOTAL:	

Received	Book Chapter
TOTAL:	

Patents Submitted

Patents Awarded

Awards

1st Place, Student Presentation at Summer Undergraduate Research Institute 2013, Kahla Haines
3st Place, Student Presentation at Summer Undergraduate Research Institute 2013, Susan Njoki
2st Place, Student Presentation at Summer Undergraduate Research Institute 2014, Susan Njoki

Graduate Students

NAME	PERCENT_SUPPORTED	Discipline
Xuan Zhao	1.00	
FTE Equivalent:	**1.00**	
Total Number:	**1**	

Names of Post Doctorates

NAME	PERCENT_SUPPORTED
FTE Equivalent:	
Total Number:	

Names of Faculty Supported

NAME	PERCENT_SUPPORTED	National Academy Member
Changyong Qin	0.25	No
FTE Equivalent:	**0.25**	
Total Number:	**1**	

Names of Under Graduate students supported

NAME	PERCENT_SUPPORTED	Discipline
Susan Njoki	0.25	
Kahla Haines	0.25	
Juan Medina	0.25	
FTE Equivalent:	**0.75**	
Total Number:	**3**	

Student Metrics

This section only applies to graduating undergraduates supported by this agreement in this reporting period

The number of undergraduates funded by this agreement who graduated during this period: 0.00
The number of undergraduates funded by this agreement who graduated during this period with a degree in science, mathematics, engineering, or technology fields:..... 0.00
The number of undergraduates funded by your agreement who graduated during this period and will continue to pursue a graduate or Ph.D. degree in science, mathematics, engineering, or technology fields:..... 0.00
Number of graduating undergraduates who achieved a 3.5 GPA to 4.0 (4.0 max scale):..... 0.00
Number of graduating undergraduates funded by a DoD funded Center of Excellence grant for Education, Research and Engineering:..... 0.00
The number of undergraduates funded by your agreement who graduated during this period and intend to work for the Department of Defense 0.00
The number of undergraduates funded by your agreement who graduated during this period and will receive scholarships or fellowships for further studies in science, mathematics, engineering or technology fields:..... 0.00

Names of Personnel receiving masters degrees

NAME
Total Number:

Names of personnel receiving PHDs

NAME	
Xuan Zhao	
Total Number:	**1**

Names of other research staff

NAME	PERCENT_SUPPORTED
FTE Equivalent:	
Total Number:	

Sub Contractors (DD882)

Inventions (DD882)

Scientific Progress

Technology Transfer

Scientific Progress Report for Proposal 59047CHREP

08/01/2011-07/31/2014

PI, Changyong Qin, Benedict College

Co-PI, Kevin Huang, University of South Carolina

The following topics were explored by experimental and theoretical methods in the funded period of 08/2011-07/2014. A full progress report is presented here.

I Interaction of oxygen with molten carbonate

1.1 DFT study of CO_4^{2-} and CO_5^{2-} in gas phase

Using DFT/B3LYP methods, two intermediate structures, CO_4^{2-} and CO_5^{2-}, were identified and analyzed. The relevance to oxygen reduction at the presence of molten carbonate in the cathode of fuel cells was discussed. The binding energy of CO_2 to O_2^{2-} is calculated to be 143 kcal/mol. The high binding energy indicates that peroxide plays an important role in the adsorption of CO_2 and this is a key step in the reduction of oxygen in MCFCs. The formation of CO_5^{2-} from CO_3^{2-} and O_2 is exothermic, with an energy change of -24.3 kcal/mol, which is very comparable to the adsorption energy of oxygen on the surface defect sites of the LSM cathode of SOFCs. For the reaction of $2CO_3^{2-}+O_2 \rightarrow 2CO_4^{2-}$, the equilibrium constant at 873K is estimated to be 1.1 and CO_4^{2-} is thermodynamically favored intermediate in the oxygen reduction process. Through orbital analysis, it is found that the formation of CO_4^{2-} will significantly decrease the reduction potential of oxygen and should promote the ORR process in SOFCs.

More details of this part can be found in the published paper (Journal of Theoretical and Computational Chemistry). Because of the important role of CO_4^{2-} in ORR, next step will be concentrate on its diffusion in molten carbonate and adsorption to the LSM cathode surface. On the cathode surface, CO_4^{2-} will then be reduced back to CO_3^{2-} and O^{2-}. Finally, O^{2-} will be transferred to electrolyte and the ORR process is completed in the cathode of SOFC.

1.2 CO_4^{2-} in MC as reaction intermediate in oxygen reduction

In the structure of $(X_2CO_3)_4$ X=Li, Na, K, one carbonate was substituted by CO_4^{2-} and each structure was re-optimized using B3LYP/6-31G(d). The substitution of CO_4^{2-} does not significantly change the structure of cluster. The X-O distance is 1.968 Å, 2.305 Å and 2.667 Å for Li, Na and K, respectively. The Mulliken charge decreases in the order of Li, Na, K, which reflects the ionization energy of the alkali metals.

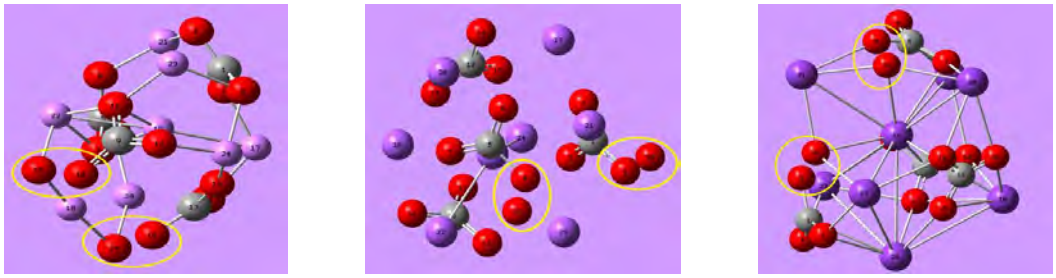

Figure 1: Structure of $(X_2CO_3)_4$ (X=Li, Na, K) with CO_4^{2-}

In this part, we are more interested in the structure of CO_4^{2-} in MC. Compared with single CO_4^{2-} calculated in the gas phase, its structure remains almost same. The O-CO_3^{2-} distance is about 1.465 Å, similar to the O-O distance in peroxide.

1.3 Oxygen reduction through CO_4^{2-} in MC

The binding of oxygen to carbonate forms CO_5^{2-}, the optimized structure of CO_5^{2-} is very close to that in gas phase reported and only negligible change was detected. This CO_5^{2-} will then react with another carbonate to form CO_4^{2-} as shown in the equations below.

$$CO_3^{2-} + O_2 \rightarrow CO_5^{2-}$$
$$CO_5^{2-} + CO_3^{2-} \rightarrow 2CO_4^{2-}$$

For step two, a transition state was located on the potential energy surface (PES) for each type of MC. IRC calculations (Figure 2) show the energy barriers and confirm the reaction path. More details will be included in the manuscript under preparation. The shift of one oxygen to the other carbonate causes the dissociation of oxygen attached to one carbonate, which makes two independent CO_4^{2-}, which then serves as oxygen carrier.

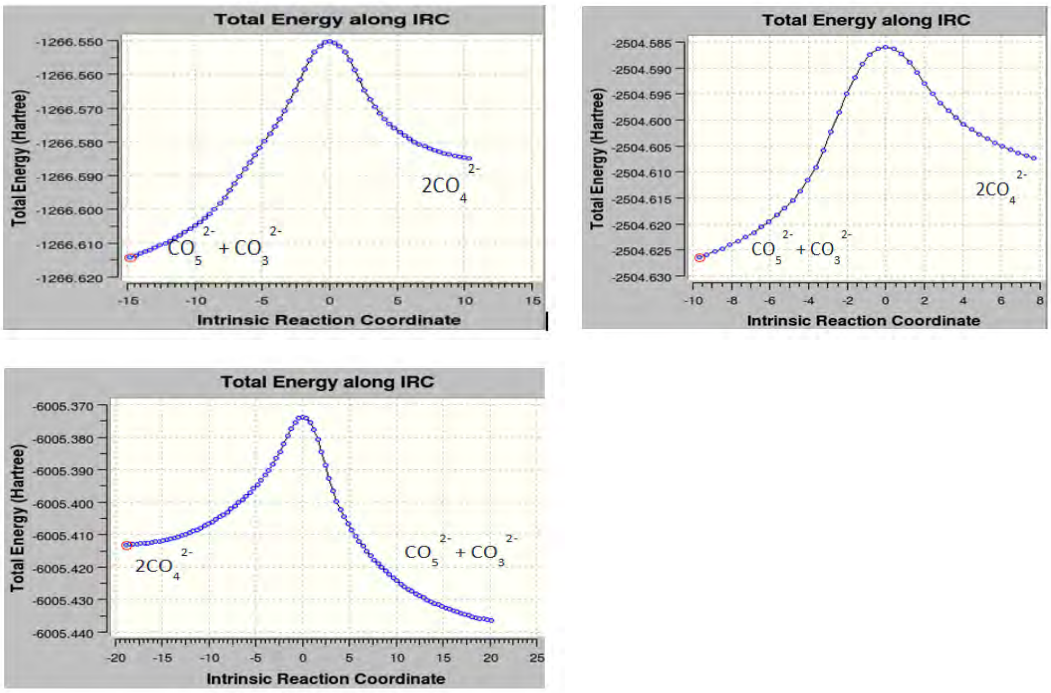

Figure 2: PES of $CO_5^{2-} + CO_3^{2-} \leftrightarrow 2CO_4^{2-}$ (Top: Li_2CO_3, Middle: Na_2CO_3, Bottom: K_2CO_3)

The energy barrier of oxygen dissociation to form CO_4^{2-} is estimated to be 49, 28, 41 kcal/mol in Li, Na, K MC, respectively. This finding needs confirmation form experiments and also further modeling with different methods will be performed to confirm if sodium carbonate will benefit the ORR process more than lithium and potassium salts.

1.4 New Oxygen Reduction Mechanism by DFT Modeling

Combining the experimental and computational results, the evidences point to that oxygen reduction is through the formation of CO_4^{2-} in MC. This active oxygen form will accept electrons and release an oxide

and carbonate. Further studies show the oxygen can easily shift between two neighboring carbonates, which means the oxygen diffusion in MC is very effective. The full reaction path is displayed in Figure 3.

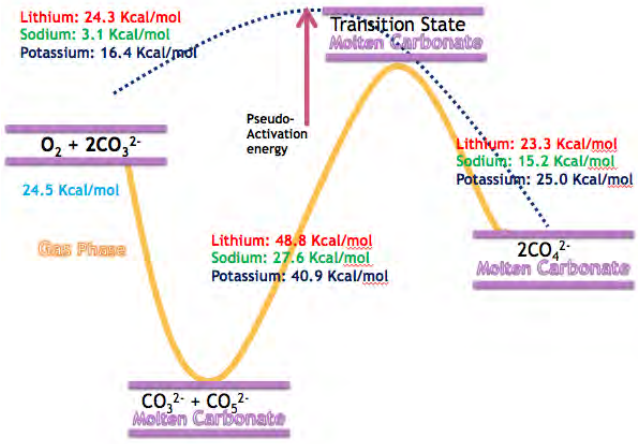

Figure 3: Formation of CO_4^{2-} by Oxygen in MC

II Fabrication and Test of SOFCs with MC Modified LSM Cathode

2.1 Fabrication

Commercial LSM powder (Nextech) was used as the cathode material. The powder was made into a paste by grinding with organic binder (V-006, Heraeus). The paste was screen printed on both sides of $La_{0.8}Sr_{0.2}Ga_{0.83}Mg_{0.17}$ (LSGM) pellets and fired at 1100 ^oC for 2 h. Li-K binary eutectic salts were prepared for infiltration. Li_2CO_3 (99%, Alfa Aesar) and K_2CO_3 (99%, Alfa Aesar) were mixed with a molar ratio of 62:38 and heated at 650 ^oC for 2 h to form a eutectic melt. In addition, eutectic melts containing 0.5 mol % La_2O_3 (99.9%, Alfa Aesar) or 0.5 mol % Gd_2O_3 (99.9%, Alfa Aesar) were also prepared. For infiltration, the eutectic melt was ultrasonic dispersed in ethanol. A few drops of the salt suspension were dripped on the surface of LSM cathodes and dried at 100 ^oC. This step was repeated till 5 mg salt was added. The samples were then heated to 650 ^oC in air for 2 h.

2.2 Electrochemical test

Silver mesh was attached to the LSM cathode using silver paste (C8829, Heraeus) for current collecting. Electrochemical Impedance Spectroscopy (EIS) of the symmetrical cells was obtained with an electrochemical workstation (IM6, Zahner) under open circuit conditions from 500 to 650 ^oC with 50 ^oC interval. The frequency range was swept from 10^5 to 0.05 Hz with an AC amplitude of 20 mV. EIS spectra were simulated and fit with Thale equivalent circuit software (Zahner). The electrode polarization was taken from the two intersections of the spectrum at the highest and lowest frequencies. Thus obtained polarization resistance was then divided by two and corrected for the cathode area to arrive at the actual area-specific resistance of the cathode polarization.

2.3 Results and Discussion

Figure 4 (a)-(d) show the polarization resistances of LSM cathode without (baseline) and with eutectic carbonate melts from 500 to 650 ^oC. The baseline LSM sample exhibits the largest polarization resistance. After infiltrated with 5 mg eutectic melts, polarization resistance has been decreased significantly. Addition of rare earth oxides La_2O_3 and Gd_2O_3 further improved the kinetics of oxygen reduction reaction. Among all the tested samples, Gd_2O_3-added Li-K carbonate melt shows the lowest area specific resistance (ASR), a 57% reduction at 650 ^oC and 80% at 500 ^oC compared to the baseline.

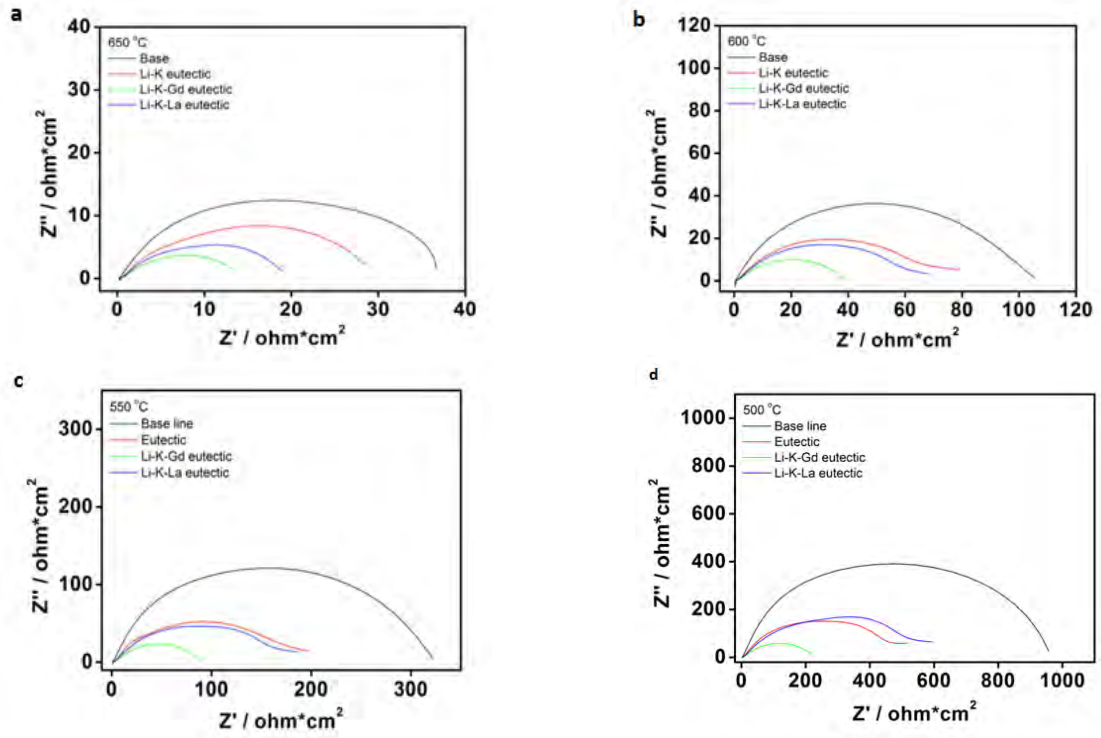

Figure 4 shows the Arrhenius plot of cathode polarization for base and eutectic melt-infiltrated LSM samples. Introduction of eutectic melts into the porous LSM cathode effectively lower the activation energy, suggesting that eutectic carbonate melts can promote the kinetics of oxygen reduction reaction

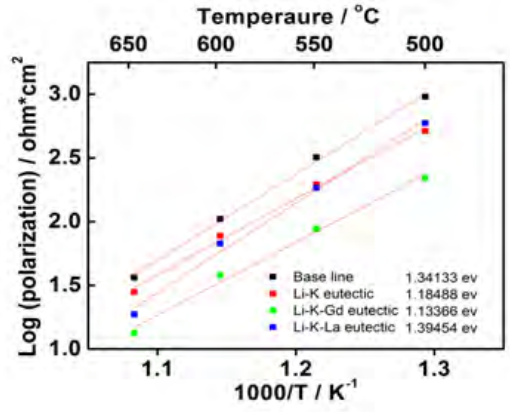

Fig.5: Temperature dependence of area-specific polarization resistance for the baseline and eutectic melt-infiltrated LSM cathode from 500 to 650 °C.

From the reported results, we can conclude: (1) Molten carbonate can improve the efficiency of LSM cathode by 50% in SOFCs; (2) Addition of MC to LSM can reduce the activation energy of oxygen reduction in the cathode of SOFCs; (3) Rare earth oxides La_2O_3 and Gd_2O_3 can also improve the cathode performance. However, the experiments could not provide any details on the fundamental steps relative to the enhancement mechanism. On the other hand, the theoretical team already proposed an oxygen reduction mechanism through CO_4^{2-} intermediate and this is consistent with the results from experiments.

III Fabrication and Test of SOFCs with MC modified LSCF/GDC Cathode

3.1 Fabrication of MC modified LSCF/GDC cathode cells

A commercial LSCF+GDC cathode pink (Sku: 232202, Fuel Cell Materials) was used to screen-print the two identical layers of porous cathode on the LSGM electrolyte. The tri-layer symmetrical cells were fired at 1100^{o}C for 1 h. The effective surface area and thickness of the resultant cathode are 0.75 cm^2 and 30 μm, respectively. For all electrochemical tests below 650^{o}C, silver paste (C8829, Heraeus) and silver mesh were used as the current collector.

A range of binary Li-K carbonate compositions was prepared by melting lithium carbonate (99%, Alfa Aesar) and potassium carbonate (99%, Alfa Aesar) at 650^{o}C for 2 hours. The resultant melts were then broken-up into micron size powders through ball milling, which were subsequently dispersed in ethanol under ultrasonic stirring to yield a suspension. A controlled amount of the suspension was then uniformly distributed over the cathode surface using a pipette, followed by drying at 100^{o}C, A final heat treatment was carried out at 650^{o}C for 2 hours to allow carbonates to further incorporate into porous cathode microstructure. The compositions of the binary Li-K carbonate melts was selected from Li/K=10/90 to 90/10 (mol%), including the eutectic composition at 62/38. Influence of MC loading on the cathode performance was also investigated as a variable.

The Li-Na-K carbonates were incorporated into in the cathode scaffold through vacuum infiltration of constituent carbonate solutions premixed in the eutectic composition of Li:Na:K=43.5:31.5:25.0 (mol%). The Li-Na-K precursor solution had a concentration of 1g/100ml. The loading of carbonate was controlled by the numbers of infiltration. After each infiltration, the samples were dried at 100^{o}C in air for 12h to evaporate the water solvent. Effect of MC loading on the cathode performance was also evaluated.

3.2 Structural characterization and cell analysis

The spectra of Electrochemical Impedance Spectroscopy (EIS) was collected from the symmetrical cells under open-circuit conditions, and further analyzed using the Thale equivalent circuit software (Zahner) to extract electrode polarization resistance by normalizing it to the actual cathode area (0.75 cm^2). Typical impedance scans were conducted at 50^{o}C interval from 650 to 550^{o}C. Twenty minutes were allowed to stabilize at each temperature before the scanning. The frequency was swept from 10^5 to 0.01 Hz with 20 mV of stimulus AC amplitude. A long-term stability of both pristine and MC-added cathodes was simultaneously evaluated for a total of 1,500 hours at 600^{o}C with a side-by-side cell arrangement.

The microstructures of cathodes in all the symmetrical impedance cells, either pre-tested or post-tested, were examined with a field-emission scanning electron microscopy (FESEM, Zeiss Ultra) equipped with an energy dispersive X-ray spectroscopy (EDS) analyzer.

The electrochemical performance was first characterized by the impedance spectra of symmetrical cells from 450^{o}C to 650^{o}C with 50^{o}C interval. The frequency was swept from 10^5 to 0.01 Hz with 20 mV of stimulus AC amplitude. Symmetrical cells with varied loading were compared in ambient condition to find out an optimized MC amount needed in cathode. The effect of oxygen partial pressure on the electrochemical performance was evaluated for the pristine and optimized cathode in the desired ratios (1atm, 0.21atm, 0.05atm and 0.001atm). A flow of 100sccm was passed over the samples at all the time and allowed to equilibrate for 20min in each atmosphere.

The same cathode was applied to the LSGM electrolyte supported full cell. This cell has an anode of Ni/GDC cermet with thickness of 50μm. For full cell test, fuel cell was sandwiched between alumina tubes sealed by low temperature glass. Voltage-current and impedance measurements were conducted from 500 to 650^{o}C with 50^{o}C interval. A H_2 flow of 50sccm and an air flow of 100sccm were supplied during the test.

The microstructure of cathode from both pristine and MC modified cells were characterized by SEM before and after electrochemical measurement.

3.3 Results and Discussion

3.3.1 The MC loading effect

The effect of MC loading into the microstructure of cathode (LSM+GDC) was evaluated using EIS technique. The EIS spectra measured in the temperature range of 500 to 650oC are shown in Fig.2. The intercept of spectra with z'-axis at high frequency represents ohmic resistance of the cell. It is evident that the presence of MC in the cathode has little effect on it. In contrast, MC has an appreciable effect on the polarization resistance of the cathode, represented by the length on the z'-axis between the high and low frequency intercepts. The results suggest that 1.3 mg/cm2 is the optimal loading for MC to yield the lowest polarization resistance.

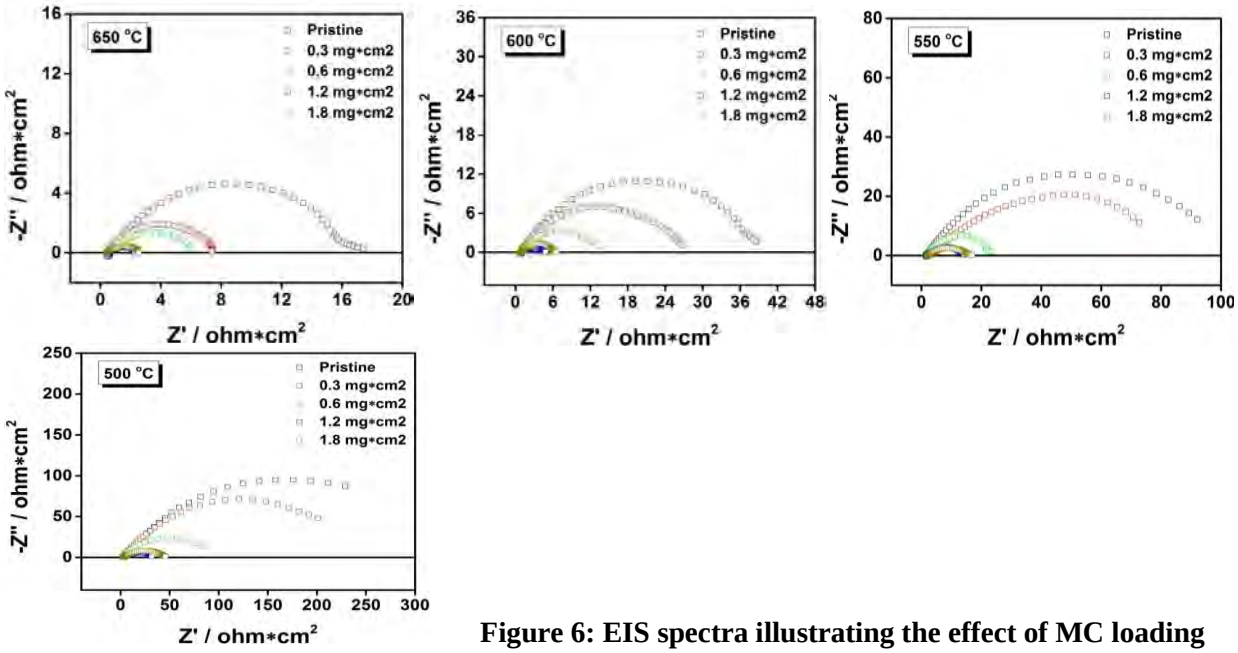

Figure 6: EIS spectra illustrating the effect of MC loading

3.2.2 The effect of partial pressure of oxygen (pO_2)

To understand the charge transfer mechanism of MC enhanced ORR, we performed EIS measurements as a function of pO_2. Fig.7 shows the EIS spectra measured as a function of temperature and pO_2 from a pristine sample. As is evident from these plots, the polarization resistance at a given temperature increases with decreasing pO_2; the ohmic resistance is little affected by the pO_2 variations. This trending suggests a *p*-type conducting behavior of the cathode. In addition, it seems that the polarization resistance is very sensitive to the change of pO_2 for this type of pristine cathode. On the other hand, the polarization resistance as well as ohmic resistance follows typical Arrhenius relationship, indicating both processes are thermally activated.

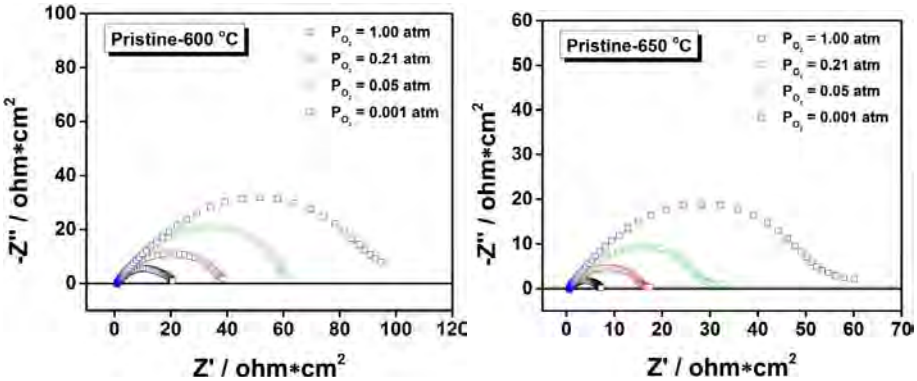

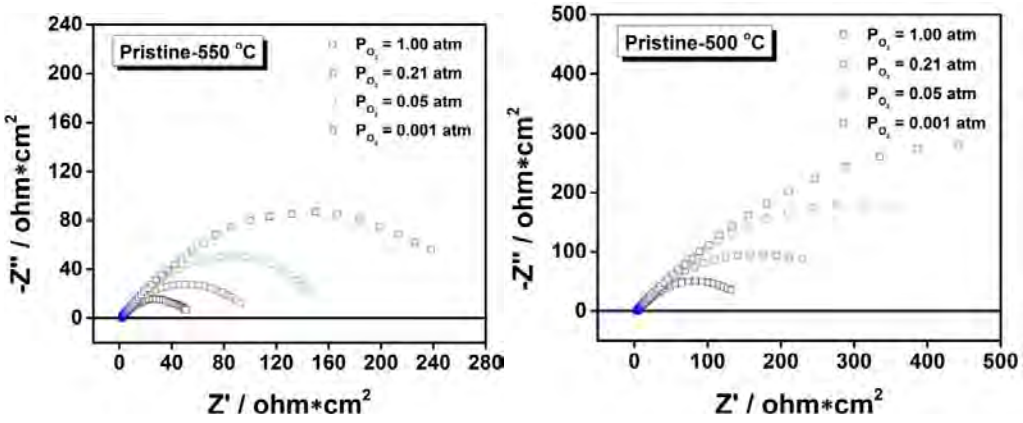

Figure 7: The ESI spectra showing the effect of pO_2 on the pristine cathode

For the MC-modified cathode, the polarization resistance shown in Fig.4 is not as sensitive to pO_2 as that of the pristine sample. The shapes of EIS spectra are also different from those of the pristine sample. These trends suggest that the charge-transfer mechanism in the MC-modified cathode is different from that in the pristine cathode.

To determine this difference, we need to construct an equivalent circuit to simulate the EIS spectra measured, from which every part of the EIS spectra is assigned with an electrochemical process. The results of the simulation can produce a series of parameters for the electrochemical processes. From these parameters, the charge-transfer mechanism can be interpreted. This part of work is currently in progress in our lab.

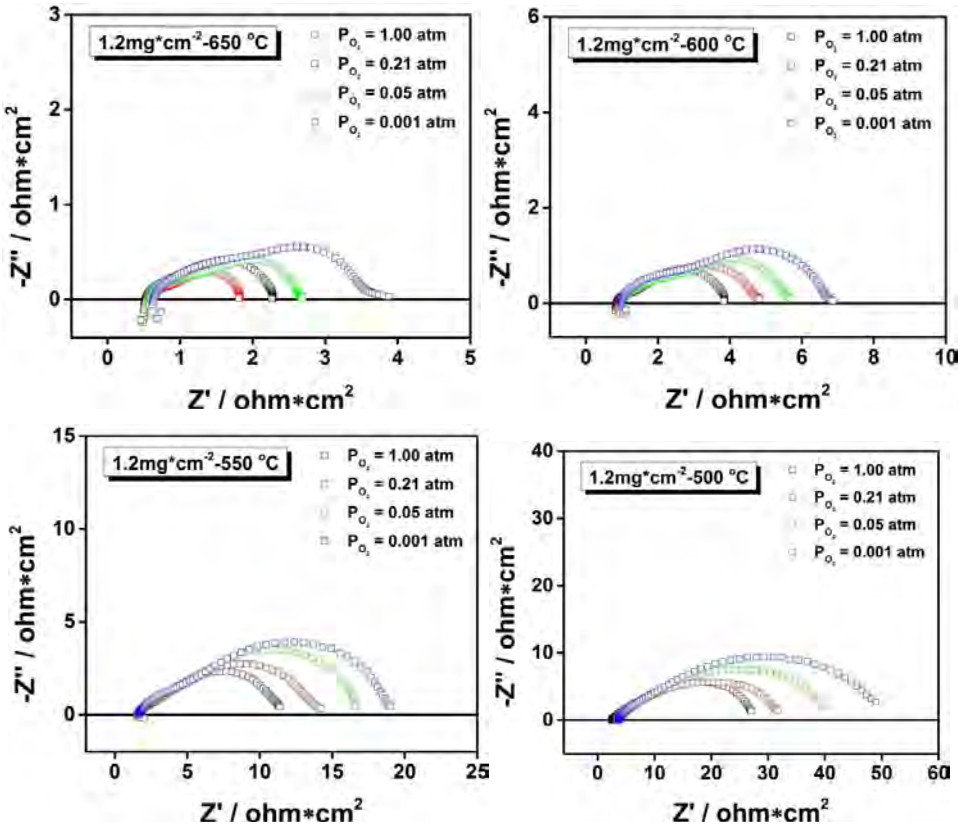

Figure 8: The ESI spectra showing the effect of pO_2 on the MC-modified cathode

3.2.3 Microstructural features

The microstructures of the pristine and MC-modified cathodes were also investigated. Fig. 9 shows the microstructures of the pristine cathode before and after the test. There is no difference discernible in the SEM images, suggesting that the microstructure of the pristine cathode has not been affected by the high temperature exposure.

The microstructures of the MC-modified cathodes shown in Fig.6 appear to be affected by the thermal exposure. Before testing, the molten morphology of MC is clearly seen in the cathode microstructure. After the test, the MC phase seems to disperse into much finer particles, spreading over the ORR active sites. The presence of MC at these active sites can promote charge transfer via oxygen absorber (CO_4^{2-}) and transporter (CO_5^{2-}).

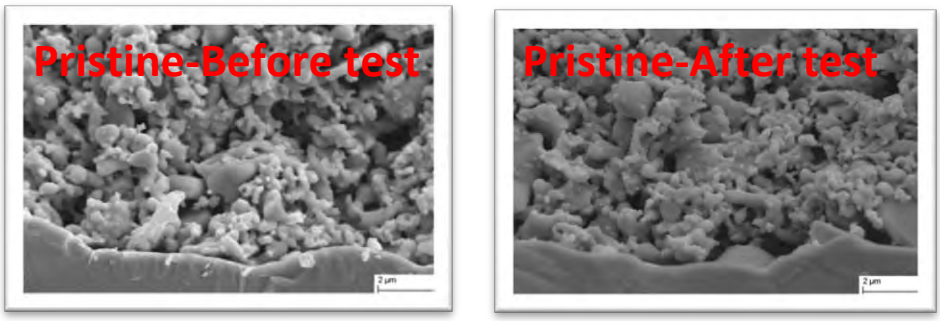

Figure 9: The SEM images of the pristine cathode before and after tests

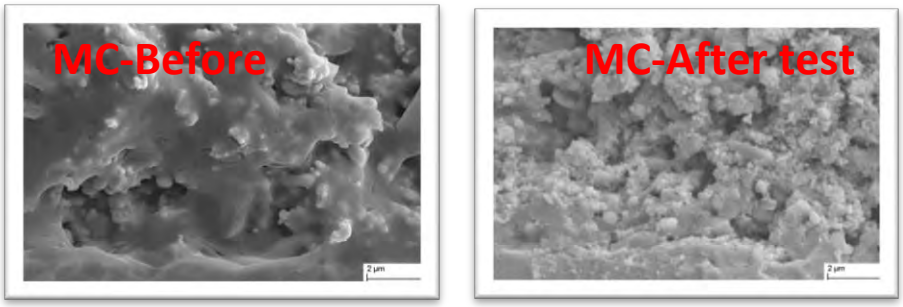

Figure 10: The SEM images of the MC-modified cathode before and after tests

3.4 Fuel cell performance

The performances measured from 500 to 650°C for SOFC with and without MC-modified cathodes are shown in Fig.11. It is evident that the presence of MC has a sizable beneficial effect on power density. At higher temperature such as 650°C, the MC-modified SOFC shows a strange behavior at high current density. We will investigate the cause behind this phenomenon.

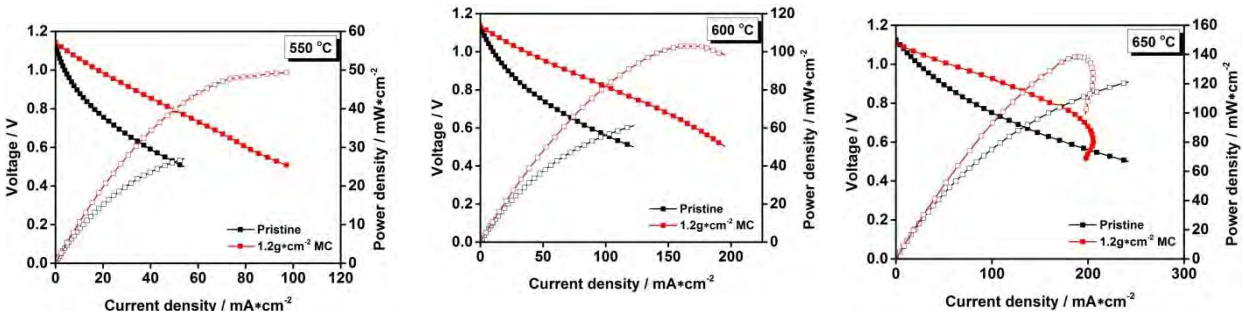

Figure 11: Comparison of V-J curves of the pristine and MC-modified SOFCs

The EIS spectra of the SOFC shown in Fig.8 further confirm the V-I results. The total cell resistance of the SOFC with MC-modified cathode clear shows a much lower value than the pristine cell.

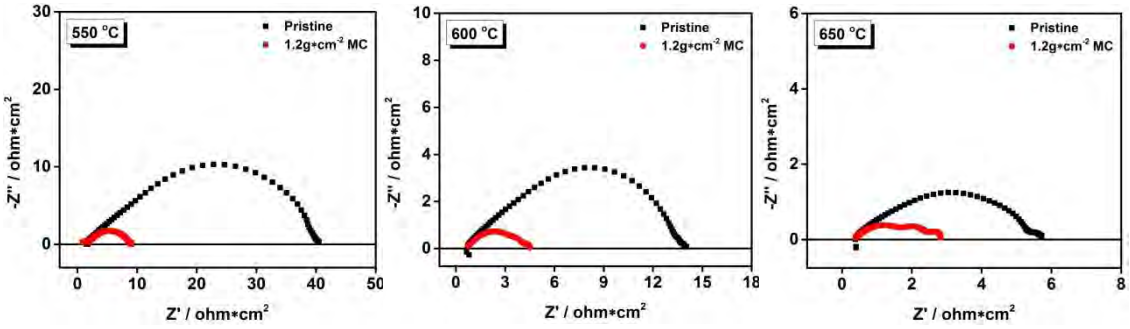

Figure 12: The ESI spectra of SOFCs with and without MC modification

IV Raman and DFT study of pyrocarbonate

4.1 In-situ Raman spectroscopic investigation

The Li_2CO_3 and Na_2CO_3 eutectic mixture (52:48 in mol%) was first synthesized in air at 650°C. After a 2-h hold, the melt was then quenched to room temperature, followed by breaking it into fine particles by ball milling. Thus prepared powders were then packed into a gold crucible that was subsequently loaded into a high temperature stage (Linkam TS1500, 0°C~1500°C). The temperature and gas were controlled by a system controller (Linkam PE95). The Raman spectra were recorded with a LabRam/HR confocal Raman system (LabRam Invers, Horiba Jobin-Yvon) with a He-Ne laser operated at 632.8 nm. Since the position of the thermal couples in the high temperature stage is located outside the crucible, the actual and the controlled temperatures of the MC are different. The melting point of the of $(Li/Na)_2CO_3$ at 490°C was used to calibrate the actual temperature. The scattering Raman spectra were collected *in-situ* from the carbonate as a function of temperature (in the range of RT- 600°C) and atmosphere (in N_2, air, CO_2).

4.2 DFT modeling

DFT calculations were performed at the B3LYP/6-31G(d) level using Gaussian09 suite of quantum programs. The geometry of $Li_2C_2O_5$ and $Na_2C_2O_5$ were optimized first, and the vibrational frequencies were then obtained from analytic second derivatives using a harmonic oscillator model. In addition, Raman intensities were computed by numerical differentiation of dipole derivatives with respect to the electric field.

4.3 Temperature dependence of Raman spectrum

Fig.1 (a) shows the Raman spectra collected from a eutectic Li_2CO_3-Na_2CO_3 (52 mol% Li_2CO_3-Na_2CO_3) melt over a band range of 650-1,850 cm^{-1} as a function of temperatures in a pure CO_2 atmosphere. For the carbonate in solid state, the Raman spectra are seen to contain four basic vibrational modes relevant to CO_3^{2-} ions. The two bands at 1,078 and 1,094 cm^{-1} are assigned to ν_1 of symmetric stretching vibrations in Li_2CO_3 and Na_2CO_3, whereas the bands at 792 cm^{-1} and 870 cm^{-1} are assigned to ν_2 of out-of-plane bending vibrations. For the isolated CO_3^{2-} that has a D_{3h} symmetry, ν_2 is Raman inactive. However, it is likely that ν_2 becomes Raman active for $(Li/Na)_2CO_3$ due to the distortion of the CO_3^{2-} structure imposed by the cations. The observed bands at 704 and 728 cm^{-1} are assigned to ν_4 of in-plane bending vibrations. This mode is a double degeneration for the distorted CO_3^{2-} induced by Li^+ and Na^+. As the CO_3^{2-} group becomes distorted from its regular planer symmetry, this mode splits into two components. The bands at 1,375 cm^{-1}, 1,404 cm^{-1}, 1,531 cm^{-1} and 1,563 cm^{-1} are attributed to a split ν_3 of the asymmetric stretching vibrations caused by the existence of Li^+ and Na^+ around the CO_3^{2-} ions.

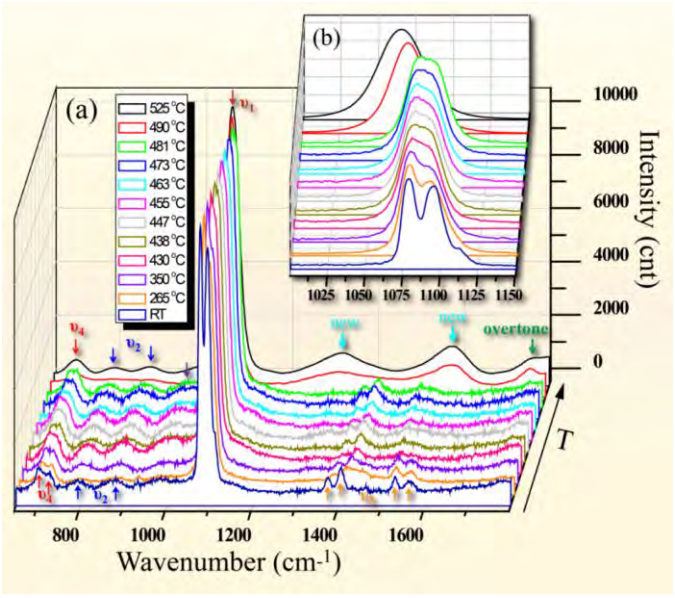

Figure 13 (a) The Raman spectra of $(Li/Na)_2CO_3$ in the region of 650-1850 cm^{-1} as a function of temperature in CO_2 atmosphere; (b) Magnified view in the region of 1,000-1,150 cm^{-1}

The shift in Raman band with temperature is better viewed in Fig.1 (b), a magnified spectrum showing the region of the major ν_1-bands at 1,078 cm^{-1} and 1,094 cm^{-1}. As the temperature increases, the ν_1-bands for Li_2CO_3 and Na_2CO_3 shift toward lower wavenumber and eventually merge into one broad peak at the melting temperature of 490°C. This shift is a direct result of lowered force-constant, elongated C-O bond length and weakened Li(Na)-C-O bond strength by increasing temperature. When the temperature reaches the melting point, the overtone of the out-of-plane bending mode ($2*\nu_2$) appears at 1,762 cm^{-1}. It should be noted that a broad but small peak near 970 cm^{-1} only observed in solid-state carbonates appears not directly related to CO_3^{2-}, identification of which is not possible for this study. We speculate that the impurities in the sample could be a source for this unknown peak. A detailed assignment of the measured Raman bands at different temperatures and atmospheres is summarized in Table 1.

The most distinguishable features of Raman spectra in Fig.1 are observed when the carbonate is in a molten state. The four bands corresponding to the ν_3 mode disappear from the spectrum while two new broad bands at 1,317 cm^{-1} and 1,582 cm^{-1} emerge within the same band width. A natural question to ask is: are these newly emerged Raman bands associated with the $C_2O_5^{2-}$ species?

Table 1 The Raman frequencies measured and assigned for the eutectic $(Li/Na)_2CO_3$ at selected temperatures and atmospheres

Atmospheres	CO_2				Air	N_2
Temperatures (°C)	RT	350	455	490 (melted)	490 (melted)	490 (melted)
Frequencies (cm^{-1}) υ_4 (weak)	704	706	706	707	707	707
	728	720	715	-	-	-
	792	790	789	790	790	790

υ_2 (weak)	879	879	881	882	885	885
υ_1 (strong)	1,078	1,077	1,077	1,070	1,072	1,072
	1,094	1,090	1,087	-	-	-
υ_3 (weak)	1,375	1,385	1,386	-	1,391	1,392
	1,404	1,415	1,416	-	1,421	1,421
	1,531	1,520	1,520	-	-	-
	1,563	1,555	1,545	-	-	-
New peaks (broad)	-	-	-	1,317 1,582	-	-
Overtone ($2*\upsilon_2$)	-	-	-	1,762	1,762	1,762
Unknown	-	-	972	-	-	-

4.4 Atmosphere-dependence of Raman spectrum

To answer this question, we first measured Raman spectra in different atmospheres. According to the enabling electrochemical reaction shown in reaction (3), the formation of $C_2O_5^{2-}$ requires a source of CO_2. Fig.2 compares the Raman spectra measured in N_2, Air and pure CO_2 atmospheres at 490°C where the carbonate is in a molten state. The bands at 1,072 cm^{-1}, 790 cm^{-1} and 885 cm^{-1}, 707 cm^{-1}, 1,391 cm^{-1} and 1,421 cm^{-1}, 1,762 cm^{-1} shown in Fig.2 (a) recorded in N_2 atmosphere correspond to the symmetric stretching (ν_1)， out-of-plane bending (ν_2), in-plane bending (ν_4), asymmetric stretching (ν_3), and the overtone of the out-of-plane bending mode ($2*\nu_2$) vibrations, respectively. The Raman spectrum in air is almost identical to that collected in N_2. However, the peaks at 1,317 cm^{-1} and 1,582 cm^{-1} shown in Fig.14 (c) are only observable in the CO_2 atmosphere.

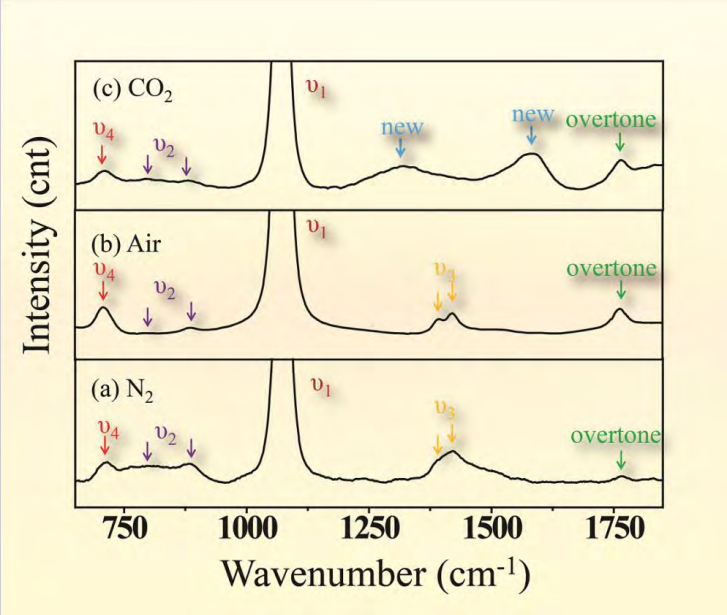

Figure 14: Raman Spectra of CO_2 in Different Atmosphere

The strong CO_2-dependence of the bands at 1,317 cm^{-1} and 1,582 cm^{-1} provides a crucial hint for the formation of $C_2O_5^{2-}$ via the CO_2 chemisorption reaction $CO_2+CO_3^{2-}=C_2O_5^{2-}$.

4.5 DFT Modeling

The theoretical support to the formation of $C_2O_5^{2-}$ is provided by the DFT calculations. The calculations indicate that high Raman activities of $C_2O_5^{2-}$ are within a band width of 1,200-1,600 cm^{-1}. Specifically, the active Raman bands are predicted at 1,366 cm^{-1}, 1,531 cm^{-1} and 1,566 cm^{-1} for $Li_2C_2O_5$ and 1,345 cm^{-1}, 1,547 cm^{-1} and 1,579 cm^{-1} for $Na_2C_2O_5$, respectively. The recorded spectrum in the band width of 1,200-1,650 cm^{-1} from the MC within 490-525°C in CO_2 atmosphere could, therefore, be an overlap of these characteristic Raman peaks of $Li_2C_2O_5$ and $Na_2C_2O_5$ in this band region. To deconvolute the two unique broad peaks around 1,317 cm^{-1} and 1,582 cm^{-1}, we used Guassian-Lorentizian function with the six theoretical Raman frequencies as the standards. The results are shown in Fig.3, where the black and red lines represent the measured and modeled spectra, respectively. Also shown are the individual spectrum calculated for the pure $Li_2C_2O_5$ and $Na_2C_2O_5$, represented by pink and blue lines, respectively. It appears that the modeled spectrum is dominated by the Na_2CO_3; only one peak at 1,566 cm^{-1} is visible for the Li_2CO_3 while the other two are too weak to be seen. This is primarily due to the differences in size and polarizability of the Na^+ and Li^+ ions. Overall, the measured Raman spectrum is in excellent agreement with the DFT calculations if the temperature effect is factored in.

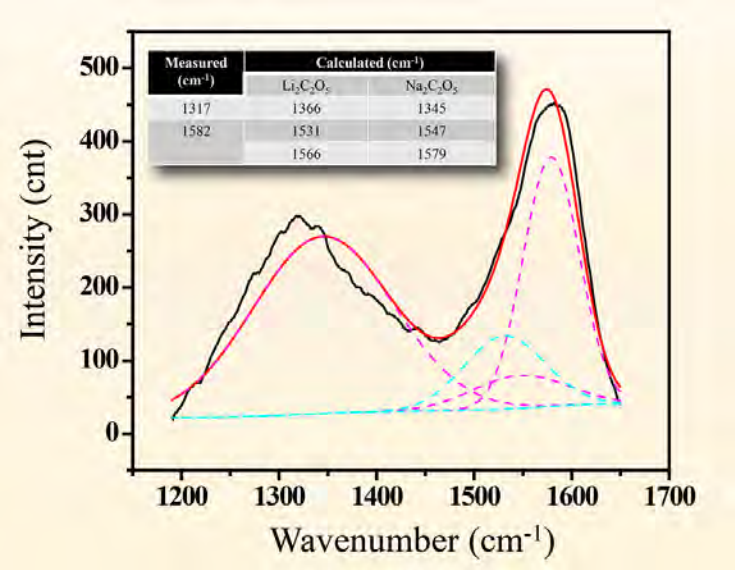

Figure 15: Deconvolution of the two broad bands observed at 1,317 cm^{-1} and 1,582 cm^{-1}; Inset: the measured and DFT-modeled Raman spectra in a band width of 1,200 - 1,650 cm^{-1}

4.6 Conclusion

In summary, we demonstrate the first experimental evidence for the existence of pyrocarbonate $C_2O_5^{2-}$ species in a eutectic Li_2CO_3-Na_2CO_3 melt exposed to CO_2 atmosphere through a combined "DFT modeling" and "Raman Spectroscopy" approach. The existence of $C_2O_5^{2-}$ species is a key support to a new bi-ionic transport model established to elucidate the fundamentals of the high-flux CO_2 transport phenomenon observed in the superior mixed oxide-ion and carbonate-ion conducting CO_2 separation membranes. The broad Raman bands centered at 1,317 cm^{-1} and 1,582 cm^{-1} are a characteristic of $C_2O_5^{2-}$ species in molten carbonates exposed CO_2 atmosphere. The measured characteristic Raman frequencies of $C_2O_5^{2-}$ are in an excellent agreement with the DFT-model consisting of six overlapping individual theoretical bands calculated from $Li_2C_2O_5$ and $Na_2C_2O_5$.